ELSEVIER

Contents lists available at ScienceDirect

Redox Biology

journal homepage: www.elsevier.com/locate/redox



A novel role for the ROS-ATM-Chk2 axis mediated metabolic and cell cycle reprogramming in the M1 macrophage polarization

Chunlu Li ^{a,b}, Chengsi Deng ^{a,b}, Siwei Wang ^{a,b}, Xiang Dong ^{a,b}, Bing Dai ^c, Wendong Guo ^{a,b}, Qiqiang Guo ^{a,b}, Yanling Feng ^{a,b}, Hongde Xu ^{a,b}, Xiaoyu Song ^{a,b}, Liu Cao ^{a,b,*}

ARTICLE INFO

Keywords: Macrophage ROS Chk2 PKM2 p21

ABSTRACT

Reactive oxygen species (ROS) play a pivotal role in macrophage-mediated acute inflammation. However, the precise molecular mechanism by which ROS regulate macrophage polarization remains unclear. Here, we show that ROS function as signaling molecules that regulate M1 macrophage polarization through ataxia-telangiectasia mutated (ATM) and cell cycle checkpoint kinase 2 (Chk2), vital effector kinases in the DNA damage response (DDR) signaling pathway. We further demonstrate that Chk2 phosphorylates PKM2 at the T95 and T195 sites, promoting glycolysis and facilitating macrophage M1 polarization. In addition, Chk2 activation increases the Chk2-dependent expression of p21, inducing cell cycle arrest for subsequent macrophage M1 polarization. Finally, Chk2-deficient mice infected with lipopolysaccharides (LPS) display a significant decrease in lung inflammation and M1 macrophage counts. Taken together, these results suggest that inhibiting the ROS-Chk2 axis can prevent the excessive inflammatory activation of macrophages, and this pathway can be targeted to develop a novel therapy for inflammation-associated diseases and expand our understanding of the pathophysiological functions of DDR in innate immunity.

1. Introduction

Macrophages, critical innate immune cells known for their remarkable plasticity, play a pivotal role in maintaining tissue homeostasis [1–3]. The uncontrolled release of inflammatory mediators and excessive oxidative stress triggered by excessive activation of macrophages are the main causes of acute inflammatory diseases such as acute respiratory distress syndrome, liver and kidney failure, and sepsis [4–7]. During acute inflammation, a substantial accumulation of ROS occurs in the process of macrophage polarization [8]. ROS is involved in several immune regulation activities, such as signal transduction, redox reactions, and autophagy [9]. Concurrently, ROS acts as a critical mediator of macrophage functional dynamics [10,11]. Microbial pathogens or their associated molecules also induce ROS production, which directly or indirectly triggers the formation of DNA double-strand breaks and contributes to immune activation [12]. The multifunctional Chk2 has a central role in the DNA damage response and is involved in

regulating the cell cycle, maintaining cellular stemness, and facilitating autophagy [13,14]. However, the role of Chk2 in immune regulation, specifically its impact on macrophage polarization, remains unknown.

In the course of oxidative stress, the generation of ROS is typically closely linked to cellular metabolic pathways [15–17]. Alterations in cellular metabolic pathways, as a consequence of immune system activation, hold paramount significance in fostering the differentiation and maturation of immune cells. During the polarization of macrophages to the M1 phenotype, there is typically an increase in glycolytic activity [18,19]. Inhibition of glycolysis can ameliorate the inflammatory response and pulmonary injury in ALI murine models [20]. Pyruvate kinase M2 (PKM2) is a crucial rate-limiting enzyme in the glycolytic pathway, playing a significant role in metabolic reprogramming and inflammatory cascades [21]. However, the mechanism by which PKM2 modulates macrophage M1 polarization remains unclear.

Macrophages stimulated with lipopolysaccharide (LPS) or IFN- $\!\gamma$ show an increase in the expression of p21, an inhibitor of cyclin-

^a The College of Basic Medical Science, Health Sciences Institute, China Medical University, Shenyang, Liaoning Province, China

b Key Laboratory of Cell Biology of Ministry of Public Health, Key Laboratory of Medical Cell Biology of Ministry of Education, Key Laboratory of Precision Diagnosis and Treatment of Gastrointestinal Tumors of Ministry of Education, Liaoning Province Collaborative Innovation Center of Aging Related Disease Diagnosis and Treatment and Prevention, China Medical University, Shenyang, Liaoning Province, China

^c Department of Pediatrics, Shengjing Hospital of China Medical University, Shenyang, Liaoning Province, China

^{*} Corresponding author. The College of Basic Medical Science, Health Sciences Institute, China Medical University, Shenyang, Liaoning Province, China. *E-mail address:* lcao@cmu.edu.cn (L. Cao).

dependent kinase 2 (CDK2) and a vital protein involved in G1/S cell cycle regulation. The increase in p21 induces cell cycle arrest and facilitates macrophage polarization [22,23]. However, the factor that triggers the p21-mediated inflammatory response during macrophage polarization remains unknown.

Macrophages respond to various external stimuli through complex and interrelated metabolic processes, including proliferation, activation, and apoptosis. M1 polarization of macrophages involves a complex interplay of cell cycle arrest and significant shifts in cell metabolism. In this study, we identified ROS as the initial driving signal for the activation of M1 polarization of macrophages. ROS amplifies glycolytic responses by inducing Chk2-mediated phosphorylation of PKM2 and concurrently induces cell cycle arrest through the accumulation of p21. This combined activity promotes macrophage polarization to a proinflammatory M1 phenotype. Our work suggests the possibility of targeting the ROS-Chk2 axis to inhibit inflammatory responses, which could lead to development of a novel therapeutic strategy for inflammatory diseases.

2. Results

2.1. ROS-ATM-Chk2 axis is involved in the M1 polarization of macrophages

We first investigated the molecular mechanisms effected by ROS production. M1 polarization of macrophages triggered by LPS and IFN- γ stimuli correlated with an increase in ROS production. The administration of antioxidant N-acetyl cysteine (NAC) counteracted this increase in ROS generation (Fig. 1A–B). The ROS signaling cascade activates the classical DNA damage response (DDR) pathway, specifically the ATM–Chk2 axis. NAC or Chk2 inhibitor treatment significantly inhibited the activity of Chk2 in macrophages with LPS and IFN- γ stimulation (Fig. 1D–F). However, phosphorylated and activated Chk2 was not localized within the cell nucleus (the site of classical DDR response) during the M1 polarization of macrophages. Instead, it could be localized in the cytoplasm (Fig. 1C), suggesting that Chk2 may have distinct physiological functions in macrophage-mediated immune responses.

To further elucidate the role of Chk2 in macrophage M1 polarization, we isolated murine bone marrow-derived macrophages (BMDMs). We found that compared to wild-type (WT) BMDMs, Chk2-deficient (Chk2-/-) BMDMs and Chk2 inhibitor-treated wild-type BMDMs demonstrated decreased activation of ERK1/2 and NF-kB signaling pathways after LPS and IFN-γ stimulation (Supplementary Figs. 1D-E). Analysis of the changes in the M1 polarization of macrophages using flow cytometry revealed that Chk2-/- BMDMs showed reduced polarization toward the M1 phenotype compared with wild-type BMDMs with LPS and IFN-γ stimulation (Fig. 1G). Similarly, polarization toward the M1 phenotype was significantly diminished when BMDMs were pretreated with NAC or Chk2 inhibitor (Fig. 1H). Furthermore, the mRNA levels of pro-inflammatory factors (IL-1β, TNF-α, IL-6, and Nos2) decreased in BMDMs pretreated with NAC or Chk2 inhibitor and Chk2-/- BMDMs (Supplementary Figs. 1F-I). In contrast, the levels of anti-inflammatory factors (IL-10 and Arg1) increased in these BMDM groups (Supplementary Figs. 1J-K). We also subjected macrophages to typical DNA damage agents, Doxorubicin and Cisplatin, as controls. Doxorubicin induces DNA double-strand breaks, activating the ATM-Chk2 pathway. While Cisplatin induces DNA single-strand breaks, activating the ATR-Chk1 pathway [24-26]. Notably, M1 polarization in macrophages occurs only when DNA damage agents activate Chk2 (Supplementary Fig. 2A-B). Collectively, these findings suggest the critical role of ROS-mediated Chk2 activation in promoting the polarization of macrophages toward the M1 phenotype.

2.2. Chk2 phosphorylates PKM2

We conducted mass spectrometry analysis of purified Chk2 protein fractions to elucidate the specific molecular mechanism by which Chk2 regulates macrophage M1 polarization. PKM2 was identified as a potential interacting protein that binds to Chk2 upon LPS stimulation (Supplementary Fig. 3A). Subsequently, co-immunoprecipitation analvsis validated the Chk2-PKM2 interaction in THP-1 cells (Fig. 2A-B). And this interaction between Chk2 and PKM2 can also be detected in BMDMs (Supplementary Fig. 3B). GST-pull down assays confirmed a direct interaction between Chk2 and PKM2 (Fig. 2C-D). Immunofluorescence staining also indicated an increase in the colocalization of Chk2 and PKM2 in macrophages with LPS and IFN-γ stimulation (Fig. 2E–F). Furthermore, the colocalization pattern of these two proteins showed a defined pattern, suggesting they may be colocalized on the endoplasmic reticulum (ER). Indeed, we found that Chk2 and PKM2 coimmunoprecipitated with the endoplasmic reticulum marker protein ERp72 (Supplementary Figs. 3C-D). Additionally, upon conducting cell fractionation to isolate the ER for immunoprecipitation experiments, we detected protein interaction between Chk2 and PKM2 on the ER (Supplementary Fig. 3E). Immunofluorescence assays validated the primary colocalization of Chk2 and PKM2 within the cytoplasmic endoplasmic reticulum in activated macrophages (Supplementary Fig. 3F). LPS stimulation enhanced the interaction between Chk2 and PKM2 during macrophage M1 polarization, and treatment with NAC or Chk2 inhibitor inhibited this interaction (Fig. 2G-H).

Then, we conducted in vitro Chk2 kinase assays to assess the potential serine/threonine kinase activity of Chk2. Our results showed that Chk2 phosphorylates PKM2 at threonine residues and not at serine residues (Fig. 2I). Moreover, LPS stimulation increased Chk2-mediated threonine phosphorylation of PKM2 in THP-1 cells. This increase was significantly reduced by treatment with NAC or Chk2 inhibitor (Fig. 2J–K). These results strongly indicate that PKM2 is a direct target of the Chk2 kinase.

2.3. Chk2-mediated PKM2 phosphorylation regulates glycolysis in macrophages to promote M1 polarization

In order to determine the PKM2 site that is phosphorylated by Chk2, we performed phosphorylation site mass spectrometry analysis. Phosphorylation site identification suggested that T95 and T195 are the potential threonine residues on PKM2 phosphorylated by Chk2 (Fig. 3A). Interestingly, these two sites on PKM2 are highly conserved across different species (Fig. 3B).

To confirm T95 and T195 sites as key targets of phosphorylation, we substituted threonine (T) with alanine (A) at T95 or T195 and performed immunoprecipitation analyses. Substituting threonine (T) with alanine (A) at T95 or T195 decreased PKM2 phosphorylation. Furthermore, the phosphorylation of PKM2 was substantially reduced in the T95/195A double mutant (2T) (Fig. 3C). The classical Y105 site on PKM2, which is closely associated with the Warburg effect, did not show significant phosphorylation changes in the early phase of macrophage polarization (Supplementary Fig. 4A). However, a decrease in glycolytic capacity was observed during the early stages of macrophage M1 polarization in BMDMs treated with NAC/Chk2 inhibitor or in Chk2-/- BMDMs (Supplementary Figs. 4B-C). Overall, our findings suggest that modifications in Chk2-mediated phosphorylation of PKM2 could be a key factor in metabolic reprogramming during the early stages of macrophage polarization.

We next attempted to validate whether the two novel Chk2-phosphorylated sites on PKM2 are involved in regulating macrophage metabolic reprogramming. To this end, we overexpressed adenovirus vectors carrying PKM2 wild-type (Ad-PKM2-WT), PKM2-T95A (Ad-PKM2-T95A), PKM2-T195A (Ad-PKM2-T195A), and PKM2-T95/195A (Ad-PKM2-2T) constructs in human macrophages. We then stimulated these macrophages with LPS and IFN- γ to induce M1 polarization.

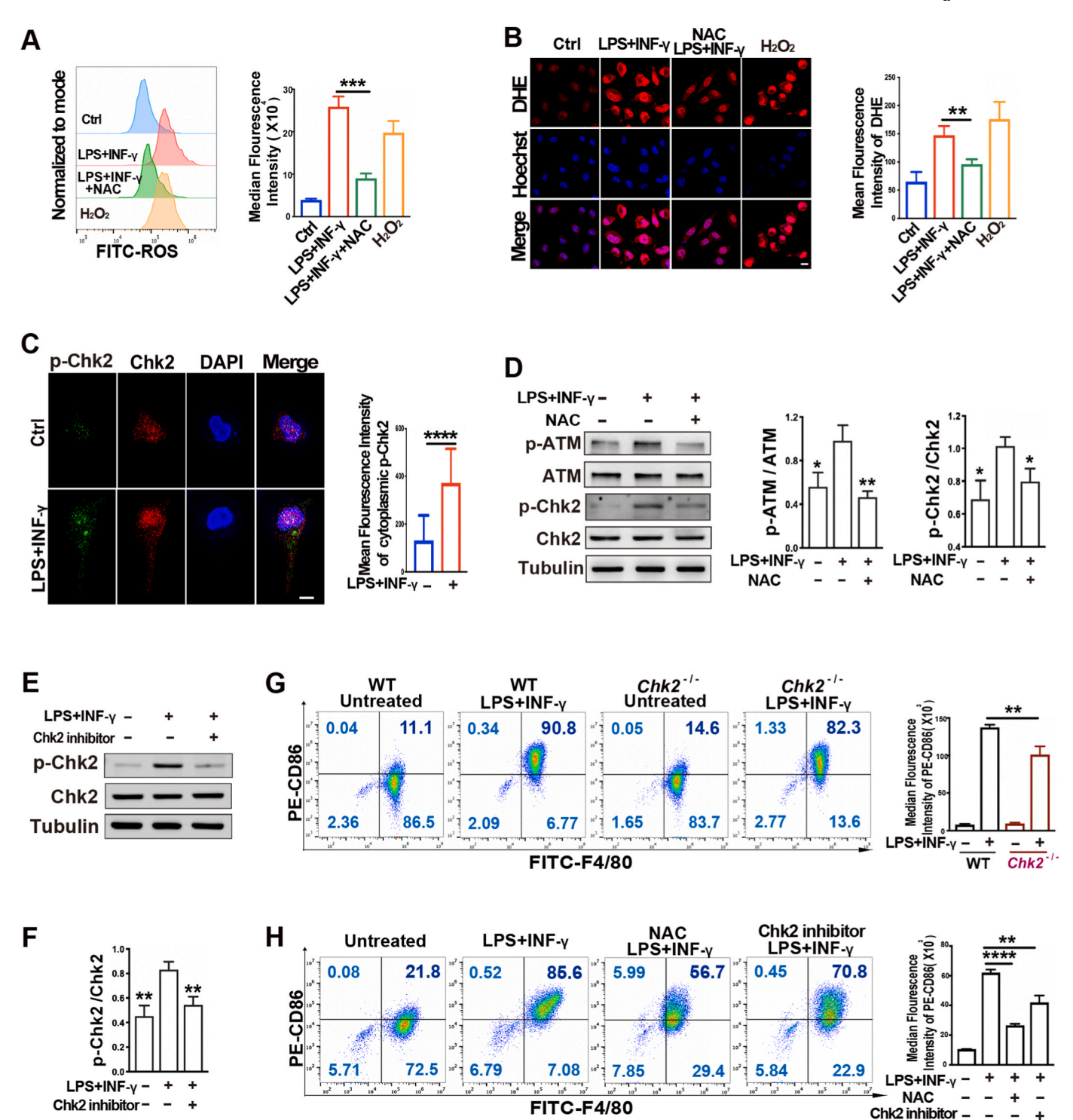


Fig. 1. ROS–ATM-Chk2 axis is involved in the M1 polarization of macrophages (A) Flow cytometric analysis of macrophages intracellular ROS levels and median fluorescence intensity of ROS expression. (n=3). (B) Representative fluorescence microscopy images and quantification of DHE. Scale bars: 5 μm (n=8). (C) Representative images of immunofluorescence staining with p-Chk2, Chk2 and DAPI in human macrophages. And mean fluorescence intensity of cytoplasmic p-Chk2 (100 cells) from three independent experiments. Scale bars: 5 μm. (D)Western blot detection of p-ATM, ATM, p-Chk2 and Chk2 in LPS/IFN-γ-stimulated human macrophages pretreated with or without NAC. Quantification of p-ATM/ATM and p-Chk2/Chk2 (n=3). (E-F) Western blot detection of p-Chk2 and Chk2 in LPS/IFN-γ-stimulated human macrophages pretreated with or without Chk2 inhibitor. Quantification of p-Chk2/Chk2 (n=3). (G) Left, representative flow cytometry plots showing the expression of F4/80 and CD86 in WT BMDMs and Chk2-deficiene BMDMs stimulated with LPS and IFN-γ. Right, bar graphs showing the median fluorescence intensity of CD86 expression. (n=3) (H) Left, representative flow cytometry plots showing the expression of F4/80 and CD86 in BMDMs pretreated with NAC or Chk2 inhibitor prior to LPS and IFN-γ. Right, bar graphs showing the median fluorescence intensity of CD86 expression. (n=3) Data are shown as mean \pm SD; *n=30.001; ***n=30.001, ****n=30.0001.

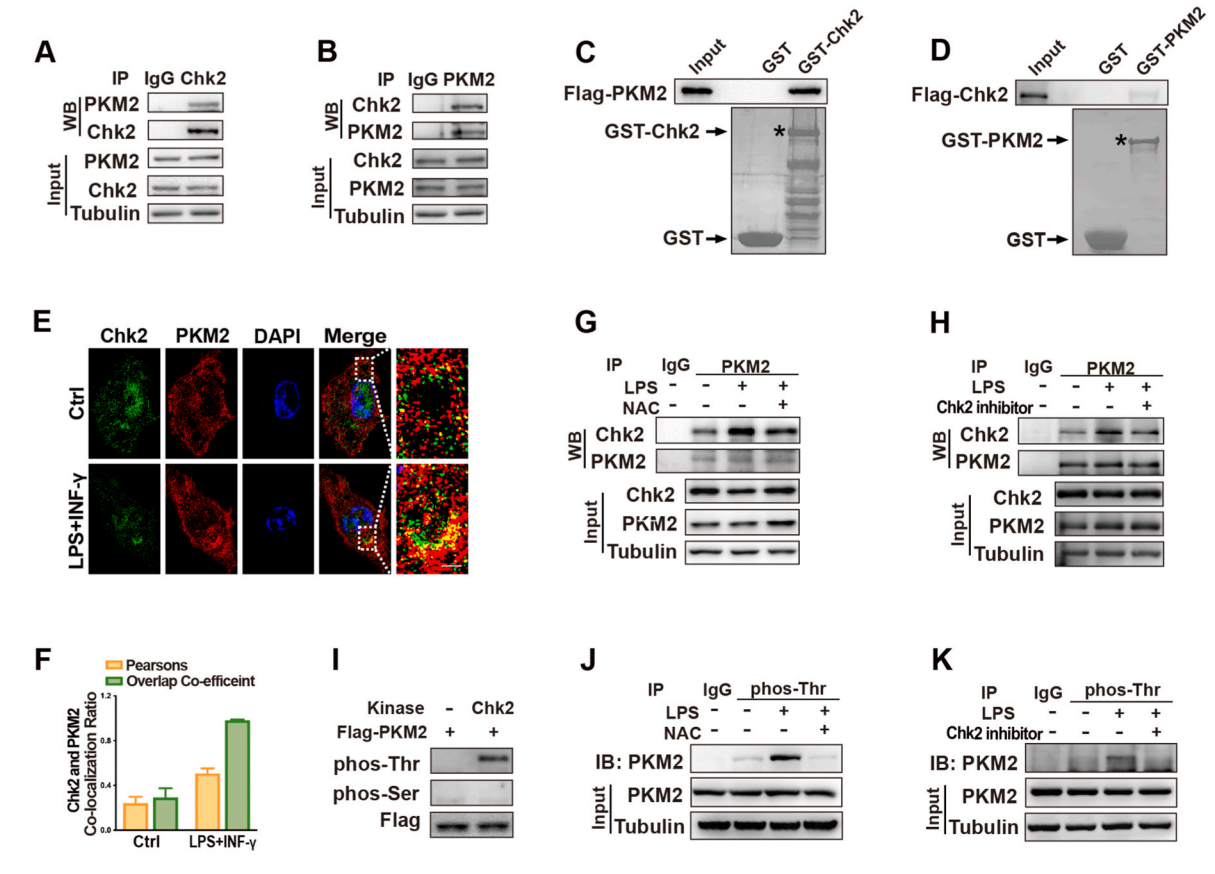


Fig. 2. Chk2 phosphorylates PKM2 (**A-B**) Co-IP showing interaction of endogenous Chk2 and PKM2 in THP-1 cells. (**C**) GST-pull down assay of Flag-PKM2 fusion proteins with bacterially expressed GST-Chk2. (**D**) GST-pull down assay of Flag-Chk2 fusion proteins with bacterially expressed GST-PKM2. (**E-F**) Localization of Chk2 and PKM2 protein in BMDMs by immunofluorescence analysis. DAPI stains cell nucleus. And the Pearson's correlation and overlap coefficient are shown in bar graph format (20 cells) from three independent experiments. Scale bar: 5 μm. (**G-H**) IP showing interaction change of Chk2 and PKM2 in THP-1 cells pretreated with NAC or Chk2 inhibitor prior to LPS. (**I**) In vitro kinase assays to test the ability of recombinant Chk2 to phosphorylate recombinant Flag-PKM2. (**J-K**) IP showing phosphorylation change of PKM2 in THP-1 cells pretreated with NAC or Chk2 inhibitor prior to LPS.

Macrophages overexpressing PKM2-T95A and PKM2-T195A showed lower extracellular lactate acidification rates compared with those overexpressing wild-type PKM2 (Fig. 3D–F). The lowest lactate acidification rate was observed in human macrophages expressing the dual-site mutation (PKM2-2T), indicating a close involvement of PKM2 T95 and T195 sites with glycolysis during macrophage M1 polarization. Metabolic reprogramming is critical in regulating macrophage polarization and function. We overexpressed Ad-PKM2-WT and Ad-PKM2-2T in BMDMs to examine their polarization toward the M1 phenotype. The attenuation of glycolysis associated with the PKM2 site mutations substantially decreased M1 polarization (Fig. 3G). Taken together, these findings confirm the involvement of the Chk2-phosphorylated PKM2 sites at T95 and T195 in regulating glycolysis and subsequently promoting the polarization of macrophages toward the M1 phenotype.

2.4. Chk2-p21 axis promotes macrophage M1 polarization

LPS stimulation induces cell cycle arrest in macrophages at the G1 phase to facilitate their polarization [27]. P21 regulates the CDK2 complex involved in the G1–S cell cycle transition and arrests the cell cycle at this phase [22]. We found that p21 expression was significantly decreased in Chk2-/- BMDMs as compared to wild-type BMDMs after LPS and IFN- γ stimulation (Fig. 4A). Similarly, p21 expression was markedly decreased in BMDMs treated with NAC or Chk2 inhibitor (Fig. 4B). Furthermore, BrdU staining results indicated that the G1-phase arrest triggered by LPS and IFN- γ was reversed in Chk2-/- BMDMs or BMDMs pre-treated with NAC or Chk2 inhibitor (Fig. 4C). In

the DNA damage response, p53 serves as a crucial link between Chk2 and p21 [28]. Upon treating macrophages with the p53 agonist nutlin-3a, a significant increase in the expression of both p53 and p21 was observed; however, M1-type polarization did not occur in macrophages (Supplementary Figs. 5A–B). Literature reports indicate that elevated p21 expression resulting from p53 activation can induce polarization of macrophages towards tumor-associated macrophages (TAMs), an M2-like macrophages [29]. Moreover, Erk1/2 is known to modulate p21 expression, influencing the G1/S cell cycle phase [30]. In our study, both Chk2-/- and Chk2 inhibitor treated macrophages exhibited a reduction in ERK1/2 phosphorylation levels (Supplementary Figs. 2A–B). Thus, our findings suggest that during the process of M1 polarization in macrophages, the regulation of p21 by Chk2 occurs independently of p53 but involves the modulation of Erk1/2 activation.

Next, we isolated p21-/- mouse BMDMs to determine the impact of p21-induced cell cycle arrest on macrophage polarization. BrdU flow cytometry analysis revealed that G1-phase cell cycle arrest was reversed in p21-/- BMDMs as compared to wild-type BMDMs after LPS and IFN- γ stimulation (Fig. 4D–E). Subsequently, macrophage polarization was compared in these two genotypes. The proportion of p21-/- BMDMs polarizing toward the M1 phenotype was significantly lower than that of wild-type BMDMs (Fig. 4F). Furthermore, the activation of Erk1/2 and NF- κ B inflammatory signaling pathways, as well as the mRNA levels of the pro-inflammatory factors IL-1 β , TNF- α , IL-6, and Nos2 were significantly decreased in p21-/- BMDMs as compared to wild-type BMDMs (Supplementary Figs. 6A–B). We also observed a decrease in the activation of the Erk1/2 and NF- κ B inflammatory signaling pathways and

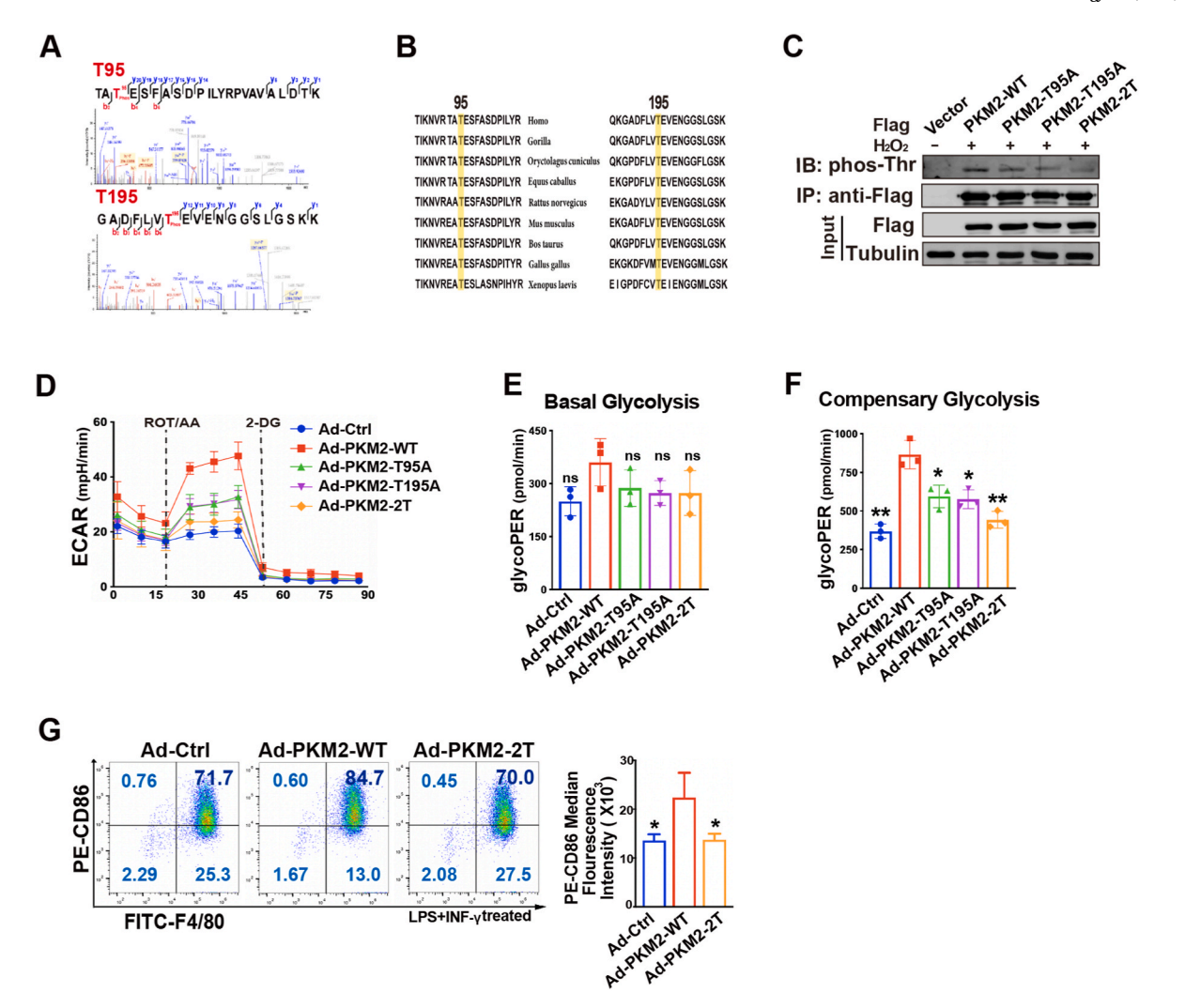


Fig. 3. Chk2-mediated PKM2 phosphorylation regulates the glycolysis in macrophages to promote M1 polarization (A) Mass spectrogram of phosphorylation sites of PKM2 protein T95 and T195. (B) Sequence alignment surrounding the T95 and T195 residue of PKM2 homologs in various species. (C) IP showing phosphorylation of PKM2 WT, T95A, T195A, and T95/195A(2T) in HCT116 cells stimulated with H_2O_2 . (D-F) Seahorse analysis of extracellular acidification rate (ECAR) in human macrophages overexpressed with PKM2 WT, T95A, T195A, and T95/195A(2T) prior to LPS and IFN- γ stimulation. (n=3) (G) Left, representative flow cytometry plots showing the expression of F4/80 and CD86 in BMDMs overexpressed with PKM2 WT and T95/195A(2T) prior to LPS and IFN- γ . Right, bar graphs showing the median fluorescence intensity of CD86 expression. (n=3) Data are shown as mean \pm SD; P>0.05 (ns, not significant), *P<0.05, **P<0.05, **P<0.01.

M1 polarization in si-p21-treated BMDMs (Supplementary Figs. 6C–D). Our results demonstrate the involvement of the Chk2-p21 axis in regulating macrophage M1 polarization in the immune response, in addition to its known role in DDR response pathway.

2.5. Inhibition of ROS-Chk2 axis protects against LPS-induced acute lung injury in mice

To further determine the role of ROS-Chk2 axis in M1 macrophage polarization in vivo, we used an LPS-induced acute lung injury (ALI) mouse model. The infiltration of M1-type macrophages was significantly reduced in the lung tissues of mice pre-fed with NAC or a Chk2 inhibitor and Chk2-/- mice compared with the respective control groups (Fig. 5A). Hematoxylin and eosin (H&E) staining revealed a significant amelioration of pulmonary inflammatory responses (Fig. 5B). Moreover, ELISA results indicated a significant decrease in the serum concentrations of IL-1 β and TNF- α (Fig. 5C-D), whereas serum IL-10 concentrations were markedly increased in Chk2-/- mice (Fig. 5E).

Considering that ROS-Chk2 signaling promoted macrophage polarization towards M1 phenotype by inducing p21 expression to arrest cell

cycle (Fig. 4F), we tested whether p21-/- mice show reduced lung inflammation. Notably, p21-/- mice infected with LPS exhibited reduced M1 macrophage infiltration and lung inflammation (Fig. 5A–B). Serum IL-1 β and TNF- α concentrations were decreased in p21-/- mice (Fig. 5C–D), while IL-10 concentrations showed no statistically significance compared with the control group (Fig. 5E).

Our data also demonstrated that Chk2-PKM2 axis is critical in regulating glycolysis to promote M1 polarization of macrophages (Fig. 3G). When we overexpressed Ad-PKM2-WT and Ad-PKM2-2T in the mouse airways and induced acute lung injury by LPS stimulation after three days, the infiltration of the M1 macrophages with PKM2 site mutations was reduced in the mouse lungs and was accompanied by a decrease in lung tissue inflammation (Fig. 5F). Peripheral blood ELISA results revealed significantly lower concentrations of the inflammatory cytokines IL-1 β and TNF- α and higher concentrations of anti-inflammatory cytokine IL-10 in Ad-PKM2-2T-infected mice compared with those in Ad-PKM2-WT-infected mice (Fig. 5G–I). Collectively, these findings confirm the ROS-Chk2 axis regulates the metabolic reprogramming and cell cycle progression to promote M1 macrophage polarization during acute inflammation.

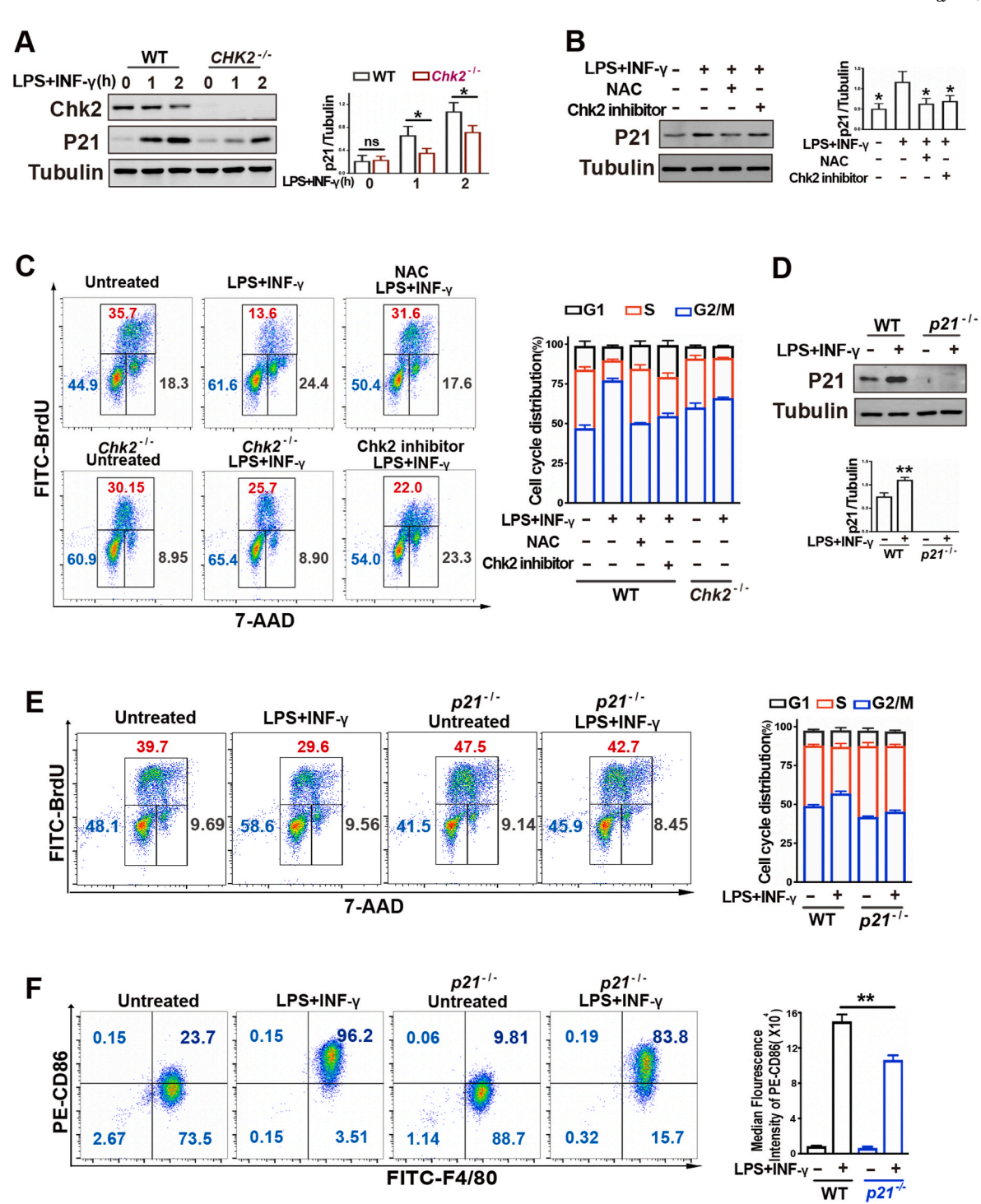


Fig. 4. Chk2–p21 axis promotes macrophage M1 polarization (A) Western blot detection of Chk2 and p21 in WT BMDMs and Chk2-deficiene BMDMs prior to LPS and IFN- γ stimulation. Quantification of p21 protein expression. (n=3) (B) Western blot detection of p21 in BMDMs pretreated with NAC or Chk2 inhibitor prior to LPS and IFN- γ stimulation. Quantification of p21 protein expression. (n=3) (C) Left, BrdU/7-AAD cell cycle analysis by flow cytometry in WT BMDMs, Chk2-deficiene BMDMs and BMDMs pretreated with NAC or Chk2 inhibitor prior to LPS and IFN- γ stimulation. Right, the quantitative cell cycle distribution data. (n=3) (D) Western blot detection of p21 in LPS/IFN- γ -stimulated WT BMDMs and p21-deficiene BMDMs prior to LPS and IFN- γ stimulation. Right, the quantitative cell cycle distribution data. (n=3) (F) Left, representative flow cytometry plots showing the expression of F4/80 and CD86 in WT BMDMs and p21-deficiene BMDMs prior to LPS and IFN- γ stimulation. Right, bar graphs showing the median fluorescence intensity of CD86 expression. (n=3)
Data are shown as mean \pm SD; P > 0.05 (ns, not significant), *P < 0.05, **P < 0.01.

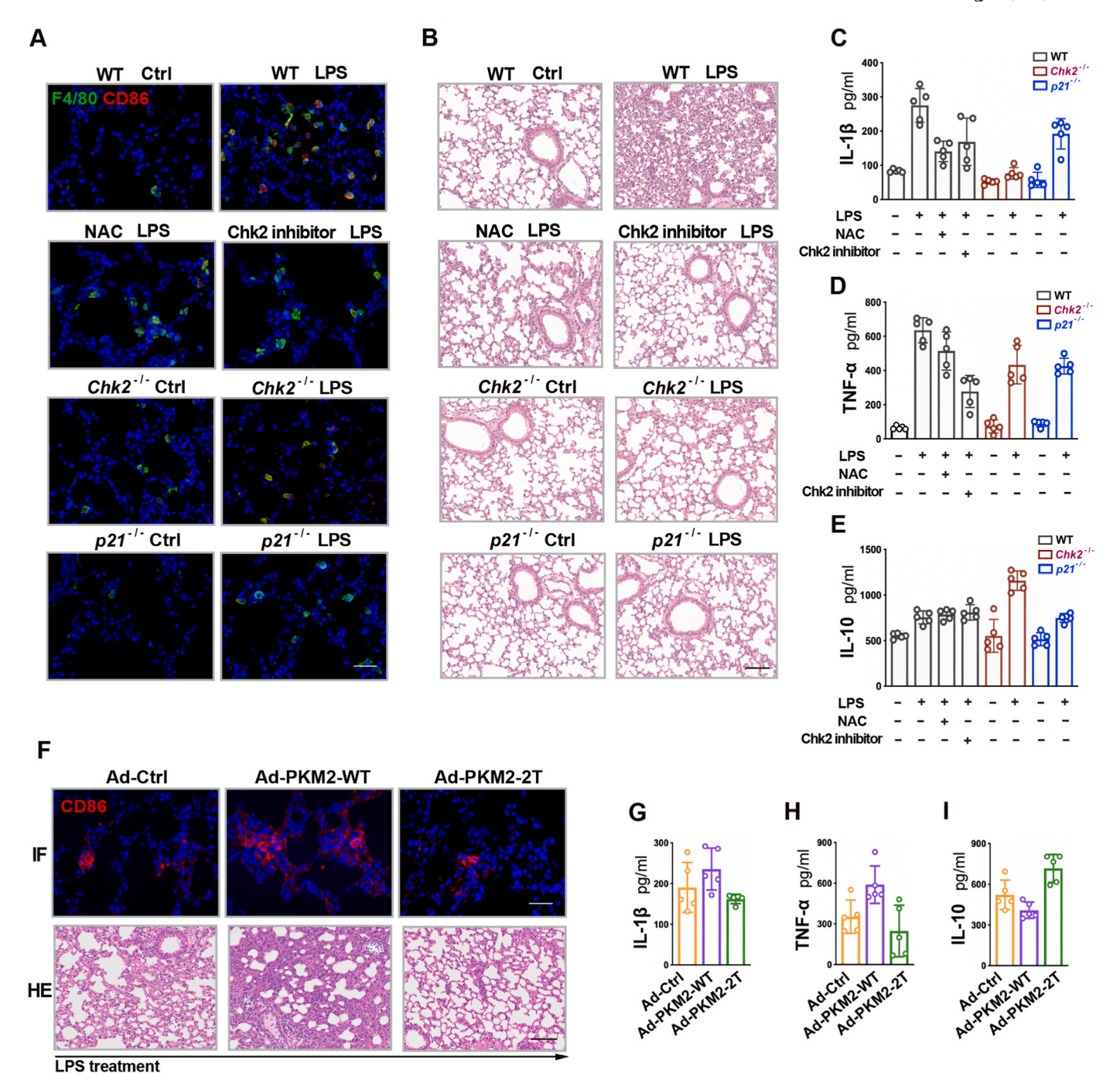


Fig. 5. Inhibition of ROS-Chk2 axis protects against LPS-induced acute lung injury in mice (A) Representative images of immunofluorescence staining with F4/80 and CD86 of murine lungs from LPS-induced WT and Chk2-/- and p21-/- mice and mice pretreated with NAC or Chk2 inhibitor prior to LPS. Scale bars: 25 μm. (B) Representative photographs of H&E staining of lungs from LPS-induced WT and Chk2-/- and p21-/- mice and mice pretreated with NAC or Chk2 inhibitor prior to LPS. Scale bars: 100 μm. (C-E) ELISA showing IL-1β, TNF-α and IL-10 levels in the serum of LPS-induced WT and Chk2-/- and p21-/- mice and mice pretreated with NAC or Chk2 inhibitor prior to LPS (n=5). (F) Upside, representative images of immunofluorescence staining with CD86 in lungs from mice overexpressed with PKM2 WT and T95/195A(2T) prior to LPS stimulation. Scale bars: 100 μm. (G-I) ELISA showing IL-1β, TNF-α and IL-10 levels in the serum of mice overexpressed with PKM2 WT and T95/195A(2T) prior to LPS stimulation (n=5).

2.6. Chk2 inhibition protects against LPS-induced post-injury lung fibrosis in mice

Pulmonary fibrosis is primarily driven by imbalanced macrophage polarization and can be categorized into three distinct pathological stages: exudative, reparative, and fibrotic phases [31,32]. M1-polarized macrophages contribute to the exudative phase. If the excessive inflammatory activation of macrophages is not suppressed, this stage can

progress into a chronic inflammatory response, leading to the development of pulmonary fibrosis [33,34].

Our animal experiments revealed that attenuating Chk2 activity markedly alleviates pulmonary inflammatory responses and reduces lung tissue damage in ALI mice. To determine whether inhibiting Chk2 activity could also mitigate pulmonary fibrotic changes resulting from lung injury, we continuously administered a low dose of LPS to both wild-type and Chk2-/- mice for three consecutive days. After 30 days,

Chk2—/— mice showed higher survival rates and greater tolerance to inflammatory responses than wild-type mice (Fig. 6A). Next, we examined the extent of pulmonary fibrosis induced by low-dose-LPS-induced lung injury. *Chk2*—/— mice and mice pretreated with NAC or Chk2 inhibitor showed a significant reduction in collagen deposition in lungs compared to wild-type mice (Fig. 6B). Moreover, the expression of fibrosis markers, namely fibronectin and vimentin, was notably diminished in lung tissues (Fig. 6C—D). Taken together, inhibiting Chk2 activity significantly ameliorated the chronic pulmonary fibrosis resulting from acute lung injury.

3. Discussion

High concentrations of ROS are generated during the progression of acute inflammation, and excessive ROS exacerbates the inflammatory response [16,35]. ROS is closely associated with the activation and function of M1 macrophages [36]. ROS is involved in activating NF-kb, MAPK and Nrf2 related inflammatory signaling pathways [37–40]. However, the underlying signaling pathways of macrophage

polarization and the complex interactions among these distinct pathways remain unclear.

Here, we discovered that ROS serves as an initiating signal, and that downstream Chk2 acts as a pivotal molecular node for cell cycle regulation and metabolic reprogramming to modulate M1 macrophage polarization. Mechanistically, Chk2 phosphorylates PKM2, enhancing glycolytic flux and promoting macrophage M1-type polarization. Additionally, we found that Chk2-dependent accumulation of p21 leads to cell cycle arrest at the G1 phase and promotes macrophage M1 polarization. Overall, we propose that the inhibition of the ROS–Chk2 pathway could be a novel therapeutic strategy for the treatment of inflammation-associated diseases.

The DDR pathway is crucial in inhibiting tumorigenesis and influences the differentiation of various cellular lineages [41–43]. This pathway primarily comprises the ATM pathway (for DNA double-strand breaks) and the ATR pathway (for DNA single-strand breaks) [44]. ATM is a vital sensor of ROS and collaborates with downstream Chk2 to suppress tumorigenesis by inducing cell senescence and apoptosis [45–47]. DDR also plays a role in innate immune responses [48,49].

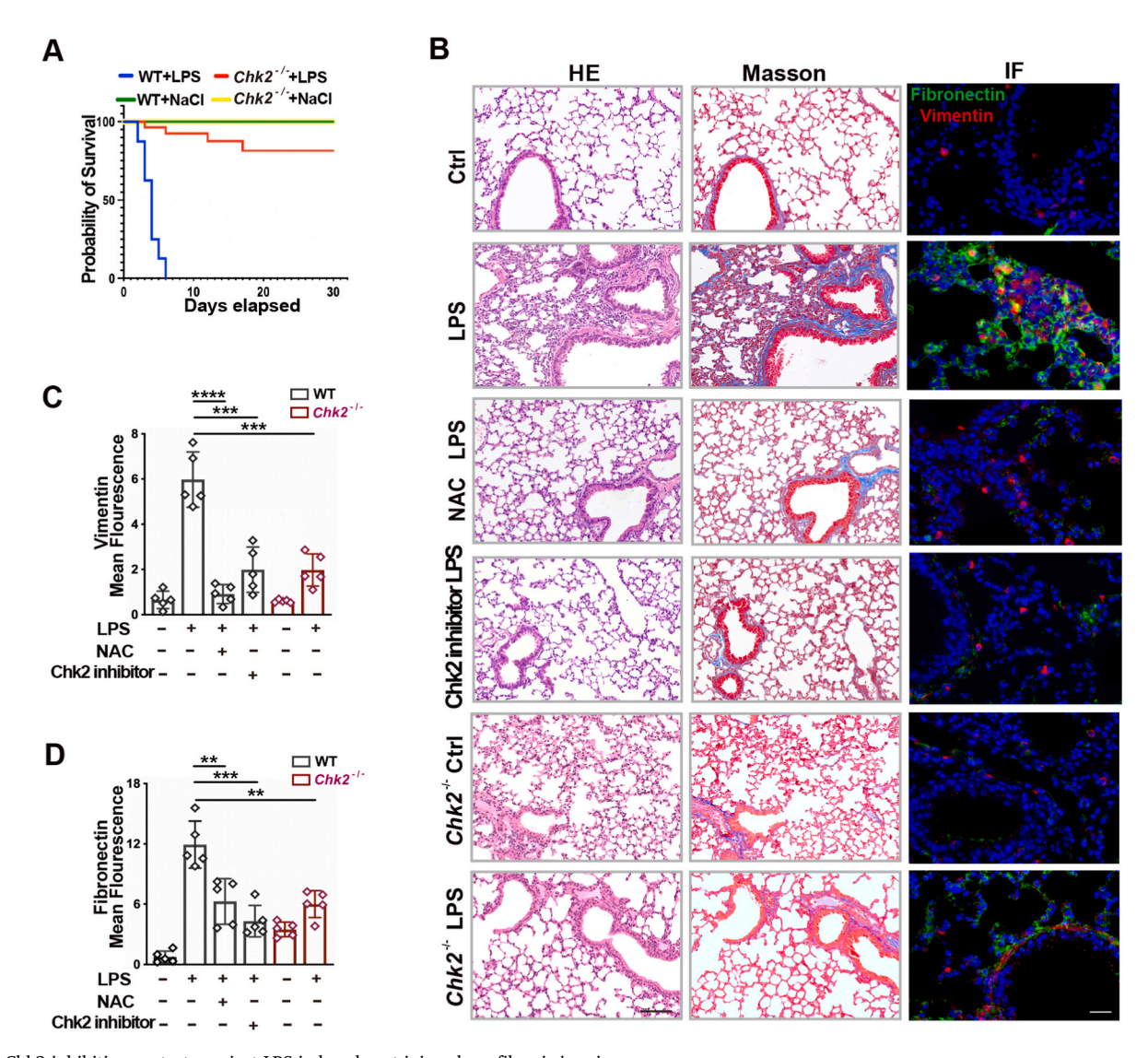


Fig. 6. Chk2 inhibition protects against LPS-induced post-injury lung fibrosis in mice (A)The Kaplan-Meier analysis log-rank test was used to estimate the survival rate of WT and Chk2-/- mice treated with or without LPS. WT + NaCl, n=6; WT + LPS, n=8; Chk2-/-+ NaCl, n=8; Chk2-/-+ LPS, n=10. (B-D) Representative images of H&E stain and Masson's trichrome stain and immunofluorescence staining with Vimentin and Fibronectin in lungs from LPS-induced WT and Chk2-/- mice and mice pretreated with NAC or Chk2 inhibitor prior to LPS. (C and D): Bar graphs showing mean fluorescence of Vimentin and Fibronectin expression in murine lungs (n=5). Data are shown as mean \pm SD; **P<0.001, ****P<0.0001.

Macrophage activation triggers ROS generation with LPS and IFN- γ exposure, directly or indirectly inducing DNA double-strand breaks. This process is associated with an increased expression of the NBS1 protein, which transports the MRN complex to the nucleus for DNA damage repair. NBS1-deficient macrophages show characteristics of senescence along with increased expression of inflammatory factors [50].

In our study, the ROS-ATM-Chk2 pathway no longer functions to sense nuclear DNA damage for repair but is instead involved in mediating the innate immune response of macrophages in the cytoplasm. We observed a decrease in glycolytic capacity and secretion of inflammatory cytokines in Chk2-deficient macrophages after stimulation with LPS and IFN-γ. Kong et al. reported that Chk2 can inhibit the nuclear translocation of PKM2 by phosphorylating its S100 site, leading to a subsequent reduction in glycolytic flux that inhibits vascular mimicry in triple-negative breast cancer [51]. Our findings indicate that activated Chk2 primarily functions in the cytoplasm, rather than the nucleus, during macrophage M1 polarization. The phosphorylation of PKM2 at the T95 and T195 sites by Chk2 promotes glycolytic reactions, facilitating metabolic shifts that contribute to macrophage activation. PKM2 forms a complex with HIF1α during inflammatory activation of macrophages and directly binds to the IL-1\beta promoter to promote its expression [52]. Moreover, inhibiting glycolytic flux using the glycolysis inhibitor 2-deoxyglucose significantly reduces the production of pro-inflammatory cytokines [53]. Here, we observed a significant reduction in the IL-1β expression in Chk2-deficient M1 macrophages. However, further studies are required to determine whether Chk2-mediated PKM2 phosphorylation affects the formation of the PKM2/HIF1 α complex in driving the IL-1 β expression. Additionally, IL-10 is an important anti-inflammatory cytokine that inhibits glycolysis and suppresses the mTOR activity [54]. Here, we found that Chk2-deficient macrophages show high IL-10 expression. However, the regulatory interplay between Chk2 and IL-10 requires further exploration.

Macrophages undergo G1 cell cycle arrest upon stimulation with LPS and IFN-7, which is characterized by upregulated expression of p21. P21 halts cell proliferation and supports cellular polarization. Therefore, p21 also participates in inflammatory modulation in addition to its classical role as a cell cycle checkpoint. P21 -/- mice are more susceptible to LPS-induced septic shock, and the absence of p21 in macrophages promotes the activation of NF-kB and the subsequent production of proinflammatory cytokines [55]. Similarly, p21-/- mice exhibit substantially increased macrophage counts and severe joint damage in a rheumatoid arthritis model [56]. However, p21 appears to play a dual role in macrophage activation. It acts as a negative regulator in some contexts, whereas it is suggested to be a positive regulator of immune activation. P21-/- mice show reduced pulmonary inflammation in response to LPS-induced pneumonia and increased resistance to transfer-induced arthritis [57,58]. In this study, p21 expression in macrophages increased in a Chk2-dependent manner after LPS and IFN- γ stimulation. Suppression of p21 expression to alleviate G1 cell cycle arrest may decrease the polarization of macrophages toward the M1 phenotype. We found that p21-deficient macrophages displayed decreased M1 polarization and reduced expression of pro-inflammatory cytokines when exposed to LPS and IFN-y stimulation. This finding contrasts with previous reports. We speculate that the age of p21-/mice during experimentation may influence their response to inflammatory stress, despite their normal development. Future studies could investigate the immune response of p21-/- mice at different ages to clarify the role of p21 in immune regulation.

Our study shows, for the first time, that immune metabolic reprogramming is interconnected with the cell cycle through Chk2, the key protein of DDR response. Our results provide a unique perspective on the role of DDR in innate immune responses. However, this study has several limitations. For example, the crosstalk between metabolic transformation and cell cycle arrest in the inflammatory activation of macrophages has not been completely elucidated. Therefore, we aim to

further explore this complex interrelationship in our future studies.

4. Materials and methods

4.1. Animals and cell culture

 $\mathit{Chk2} \pm \mathrm{and} \ \mathit{p21} \pm \mathrm{mice}$ were a kind gift from Takai H [59]. $\mathit{Chk2-/-}$ and $\mathit{p21-/-}$ mice were generated by crossing $\mathit{Chk2} \pm \mathrm{and} \ \mathit{p21} \pm \mathrm{mice}$. Male mice (8–10 weeks old) were used in this study with their age- and gender-matched littermate wild-type mice ($\mathit{Chk2+/+}$ and $\mathit{p21+/+}$) as controls. Standard PCR was used for genotyping. Mice were kept in specific pathogen-free conditions. All animal experiments were approved and performed in accordance with the guidelines of the Institutional Animal Care and Use Committee of China Medical University.

BMDMs were prepared from wild-type, Chk2-/-, or p21-/- mice by culturing the cells in Dulbecco's modified Eagle's medium with 10 % heat-inactivated fetal bovine serum, 10 ng/ml M-CSF (#SRP3221, Sigma), 100 U/ml penicillin, and 100 µg/ml streptomycin for 4–6 days. Subsequently, BMDMs were cultured in 100 ng/ml LPS (#L3012, Sigma) and 20 ng/ml IFN- γ (#315-05-20, PeproTech) for M1 polarization.

PBMCs were isolated from healthy human blood using the Mojo-SortTM human CD14 $^+$ monocytes isolation kit (#480048, Biolegend). PBMCs were cultured in RPMI 1640 medium with 10 % heat-inactivated FBS, 25 ng/ml M-CSF (#SRP3110, Sigma), 100 U/ml penicillin, and 100 µg/ml streptomycin for 5–7 days to differentiate into human macrophages. Subsequently, the macrophages were cultured in 50 ng/ml LPS and 20 ng/ml IFN- γ for M1 polarization. All experiments involving human samples were conducted in compliance with all relevant ethical regulations and were approved by the Ethics Committee of Medical Research of China Medical University.

THP-1, HEK 293, HEK 293 Cas9-Chk2 and HCT116 cells were obtained from cell bank of Cao's lab. HEK 293 and HEK 293 Cas9-Chk2 cells were cultured in DMEM medium with 10 % FBS, 100 U/ml penicillin, and 100 μ g/ml streptomycin THP-1 and HCT116 cells were cultured in RPMI 1640 medium with 10 % FBS, 100 U/ml penicillin, and 100 μ g/ml streptomycin.

4.2. Antibodies and reagents

The following antibodies were used for western blotting: anti-ATM (# 2873, CST), anti-Phospho-ATM (#13050, CST), anti-Chk2 (#6334, CST), anti-Chk2 (611570, BD Pharmingen), anti-Phospho-Chk2 (#2661, CST), anti-PKM2 (#4053, CST), anti-Phospho-PKM2 (#3827, CST), anti-p53 (#2524, CST), anti-Phospho-Threonine (#9386, CST), anti-Phospho-Serine (AB1603, Sigma), anti-p38 (#8690, CST), anti-Phospho-p38(#4511,CST), anti-Ph-kB (sc-8008, Santa Cruz Biotechnology), anti-Phospho-NF-kB (sc-136548, Santa Cruz Biotechnology), anti-ERp72 (sc-390530, Santa Cruz Biotechnology), anti-Flag-Tag (SG4110-16, Shanghai Genomics Technology), anti-Flag-Tag (SG4110-16, Shanghai Genomics Technology), anti-Flag-Actin (AC004, ABclonal), and anti-Tubulin (#2144, CST).

The following antibodies were used for immunofluorescence assays: anti-F4/80 (sc-52664, Santa Cruz Biotechnology), anti-CD86 (sc-28347, Santa Cruz Biotechnology), anti-Fibronectin (sc-8422, Santa Cruz Biotechnology), anti-Vimentin (sc-6260, Santa Cruz Biotechnology), anti-ERp72 (CL549-66365, Proteintech), anti-Phospho-Chk2 (#2661, CST), anti-PKM2 (#4053, CST), anti-Chk2 (#611570, BD Pharmingen), anti-Tubulin (#2144, CST), DAPI (#32670, Sigma).

NAC was purchased from Beyotime (#s0077). Chk2 inhibitor II (#C3742) and hydrogen peroxide solution (#323381) were purchased from Sigma. Nutlin-3a was purchased from Absin (abs813165). Doxorubicin (S1208) and Cisplatin (S1166) were purchased from Selleck.

4.3. Animal models of LPS-induced ALI and post-injury pulmonary fibrosis

Mice were intraperitoneally injected with LPS (L2630, Sigma; 10 mg/kg body weight) for 8 h to establish the ALI model. Control animals were injected with only saline. Mice in the NAC + LPS group were fed with NAC dissolved in water (1 mg/ml) for three days before LPS administration. Mice in the Chk2 inhibitor + LPS group were intraperitoneally injected with a Chk2 inhibitor (20 mM/kg body weight) 2 h before LPS administration. Ad-Ctrl, Ad-PKM2-WT, and Ad-PKM2-T95/195A (1 \times 10 9 pfu/mouse) were administered to the adenovirus gene delivery groups three days before LPS administration using intratracheal injection. Mice were anesthetized and the adenovirus was directly injected into the trachea following surgical visualization. Mice were sacrificed after 8 h, and the lung tissues and blood samples were collected under aseptic conditions.

In addition, Mice were peritoneally injected with LPS (5 mg/kg body weight) for three days to estimate the survival rate of WT and Chk2-/- mice. Mice were peritoneally injected with LPS (4.5 mg/kg body weight) for three days and observed for the next four weeks to establish the postinjury pulmonary fibrosis model. Lung tissues were collected from mice at the end of the fourth week under aseptic conditions and processed for subsequent analysis.

4.4. Plasmid constructions, transfection, and viral infection

Flag-PKM2, GST-PKM2, Flag-Chk2, and GST-Chk2 were generated in our previous studies [60]. All constructs were confirmed using DNA sequencing, and the plasmids were then transfected into cells using the jetPrime Transfection reagent (Polyplus PT-114-15). Specific siRNAs for p21 were purchased from RiboBio Co. (Guangzhou, China). The recombinant adenovirus containing the human PKM2 gene (PKM2 WT, PKM2 T95A, PKM2 T195A, and PKM2 T95/195A) and mouse PKM2 gene (PKM2 WT and PKM2 T95/195A) were purchased from GeneChem Co. (Shanghai, China).

4.5. ROS detection

For ROS detection by flow cytometry, BMDMs were pretreated with NAC (10 mM) for 4 h, then stimulated with LPS (100 ng/ml) and IFN- γ (20 ng/ml) for 4 h followed by incubation with FITC-ROS (MAK143, Sigma) at 37 °C for 45 min in the dark. BMDMs were treated with 1000 μ M H_2O_2 for 10 min as a positive control.

For ROS detection by fluorescent staining, BMDMs were pretreated with NAC (10 mM) for 4 h, then stimulated with LPS (100 ng/ml) and IFN- γ (20 ng/ml) for 4 h followed by incubation with DHE (D1168, Invitrogen) for 30 min and Hoechst (C1027, Beyotime) for 10 min at 37 $^{\circ}\text{C}$ in the dark. BMDMs were treated with 500 μM H $_2\text{O}_2$ for 30 min as a positive control.

4.6. Flow cytometry analysis

Single-cell suspensions were blocked with TruStain FcXTM (#101302, Biolegend) for macrophage M1 polarization studies. BMDMs were stained with FITC-anti-F4/80 (#301804, Biolegend), PE-anti-CD86 (#374206, Biolegend). All samples were stained for 30 min on ice in the dark, washed with PBS, and centrifuged at 300 g for 5 min. Cells were resuspended in 200 μ l PBS and analyzed using flow cytometry.

BMDMs were cultured to obtain 30 %–40 % confluence and treated with NAC (10 mM) for 4 h or Chk2 inhibitor (20 μ M) for 2 h. The cells were stimulated with LPS (100 ng/ml) and IFN- γ (20 ng/ml) for 15 min followed by adding BrdU for 45 min. Next, the cells were permeabilized, treated for 30 min with DNase, stained with FITC-BrdU and 7-AAD (#559619, BD Pharmingen) according to the manufacturer's protocols, and analyzed using flow cytometry.

4.7. Histology

Lung tissue samples were fixed in 4 % paraformaldehyde and embedded in paraffin. The tissues were cut into $4-\mu m$ thick sections, which were used for H&E and Masson's trichrome staining. Finally, the stained sections were mounted with neutral gum and analyzed using a light microscope.

4.8. Immunofluorescence

Lung tissue samples were fixed in 4 % paraformaldehyde for 4 h and transferred to a 30 % sucrose solution until the tissue settled at the bottom. The cryopreserved lung tissues were cut into 6-µm thick sections. The frozen slices were kept at room temperature for approximately 30 min before performing immunofluorescence assays. All sections were fixed in 4 % paraformaldehyde, permeabilized with 0.5 % Triton X-100, blocked with 20 % goat serum and incubated with anti-F4/80 and anti-CD86 antibodies overnight at 4 °C. Sections were washed three times with PBS and incubated with Alexa Fluor 488 goat anti-mouse IgG (A11001, Invitrogen) and red-fluorescent Alexa Fluor 594 donkey anti-rabbit IgG (A21207, Invitrogen) as secondary antibodies. The sections were again washed with PBS and stained with DAPI. Finally, the images were captured using a fluorescence microscope. Human macrophages and mice BMDMs were grown on coverslips and fixed in 4 % paraformaldehyde for 1 h at 4 °C. The rest of the procedure was like that followed for the lung sections.

4.9. ELISA

Mouse blood samples were collected, clotted, and centrifuged at 2000 rpm for 10 min. Cytokines were quantified in the serum samples using ELISA kits for mouse IL-1 β (#1210122, DAKEWE), TNF- α (#1217202, DAKEWE), and IL-10 (#1211002, DAKEWE) according to the manufacturer's protocols.

4.10. Quantitative PCR (qPCR)

BMDMs were treated with NAC (10 mM) for 4 h or Chk2 inhibitor (20 μ M) for 2 h, then stimulated with LPS (100 ng/ml) and IFN- γ (20 ng/ml) for 1 h to conduct qPCR experiment. For detection mRNA levels of inflammatory factors, Chk2-/- or p21-/- and WT BMDMs were stimulated with LPS (100 ng/ml) and IFN- γ (20 ng/ml) for 1 h to conduct qPCR experiment. Total RNA was isolated from BMDMs using the SevenFast total RNA extraction kit (SM130-02, Seven Biotech). cDNA was synthesized using the PrimeScriptTMRT reagent kit (RR037B, Takara). qPCR was performed using the TB Green Premix Ex TaqTM II kit (RR820W, Takara) on a Roche LightCycler480II system. The expression levels of each gene were normalized to GAPDH. Each experiment was performed in triplicate, and results were presented as fold change compared with the control group. The primer sets used to amplify cDNA fragments are listed in Supplemental Table 1.

4.11. Mass spectrometry

The cells overexpressing Flag-Chk2 were harvested after 48 h transfection and lysed in the immunoprecipitation lysis buffer. Flagbeads were mixed in the buffer and the resulting solution was incubated overnight at 4 $^{\circ}$ C. The solution was centrifuged, and the pellet was washed with PBS at 4 $^{\circ}$ C. Next, PBS was removed, and the beads were boiled with 2 \times loading buffer in a water bath for 10 min. The immunoprecipitated proteins were subjected to western blotting and excised from the gel for digestion and mass spectrometry analysis. Finally, standard databases were searched to identify interacting proteins and peptides.

4.12. Western blotting and immunoprecipitation

For alterations in the binding between Chk2 and PKM2, THP-1 cells were treated with NAC (20 mM) for 4 h or Chk2 inhibitor (20 μM) for 2 h, then stimulated with LPS (500 ng/ml) for 1 h. So was the same experimental condition for changes in Chk2-mediated phosphorylation of PKM2. Cells were lysed using IP lysis buffer with protease inhibitor cocktail and phosphorylation protease inhibitor, and the total cell lysates were resolved on SDS-PAGE gels. The primary antibody was added to the cell lysates and mixed by rotation for 2 h. Then, protein A/G beads (sc-2003, Santa Cruz) were added to the mixture, which was incubated at 4 $^{\circ}\text{C}$ overnight for co-IP. The samples were then washed three times with IP lysis buffer at 4 $^{\circ}$ C, and proteins were eluted with 2 \times loading buffer. The eluates were then subjected to SDS-PAGE and blotted onto nitrocellulose membranes. The membranes were blocked for 1 h at room temperature in TBST supplemented with 5 % BSA and incubated overnight at 4 °C with specific primary antibodies. The membranes were washed three times with TBST, incubated with HRP-conjugated secondary antibody at room temperature for 1 h, and then washed three times with TBST. Finally, the blots were developed using an enhanced chemiluminescence detection kit (#32106, Thermo Fisher Scientific) and analyzed using an e-Blot Western blot imaging system.

4.13. In vitro GST pull-down assay

The bacterial expression constructs (pGEX-4T-1) containing the target genes (PKM2 or Chk2) were expressed in $\it E.~coli$ BL21 cells cultured in the LB medium containing ampicillin. Cells were induced to overexpress the GST-fusion protein by adding 1 mM IPTG while shaking at 30 °C for 3 h. Next, cells were resuspended in bacterial lysis buffer followed by ultrasonication. The cell debris was then removed by centrifugation at 4 °C and 15,000 g for 5 min. The proteins were purified using glutathione-agarose beads according to the manufacturer's instructions. Flag-tagged PKM2 or CHK2 proteins were synthesized using TNT quick coupled transcription/translation kits (Promega, L1170) followed by incubation in binding buffer for 4 h at 4 °C. The samples were then washed three times with binding buffer and eluted with 2 × loading buffer. The eluates were subjected to SDS–PAGE, and protein bands were detected using western blotting.

4.14. In vitro CHK2 kinase assay

Recombinant Chk2 (200 ng) was incubated with purified Flag-tagged PKM2 protein in a kinase buffer [50 mM HEPES (pH 7.4), 10 mM MgCl2, 10 mM MnCl2, 0.2 mM DTT containing 100 μ M ATP per reaction] for 45 min at 30 $^{\circ}$ C. Phosphorylated proteins were separated using SDS–PAGE and further analyzed using mass spectrometry for phosphorylation site identification.

4.15. Metabolic flux analysis

The real-time extracellular acidification rate was measured using a Seahorse XFe24 analyzer (Agilent Technologies). Human macrophages were transduced in quintuplicates with Ad-Ctrl, Ad-PKM2-WT, Ad-PKM2-T95A, Ad-PKM2-T195A, or Ad-PKM2-T95/195A at a multiplicity of infection of 1000 for 24 h and further stimulated with LPS (50 ng/ml) and IFN- γ (20 ng/ml) for 6 h at 37 °C with 5 % CO2. BMDMs were pretreated with NAC (10 mM) for 4 h or Chk2 inhibitor (20 μ M) for 2 h. The pretreated BMDMs were stimulated with LPS (100 ng/ml) and IFN- γ (20 ng/ml) for 6 h at 37 °C with 5 % CO2. Approximately 8 \times 10 4 cells per well were seeded onto XF24 cell culture microplates using Cell-Tak. XF RPMI or DMEM medium (1 mM pyruvate, 2 mM glutamine, and 10 mM glucose) was then added into each well, and the plates were incubated at 37 °C for 30 min. The rate of glycolysis was determined using the Seahorse XF Glycolytic Rate Assay Kit (#103344-100, Agilent Technologies) according to the manufacturer's protocols.

4.16. Statistical analysis

Statistical analyses were performed using GraphPad Prism 9 software (GraphPad Software, Inc.). Data were presented as mean \pm SD from 3 independent experiments. P-values $<\!0.05$ were considered statistically significant. Statistical analyses were performed using Student's t-test for the comparison of two groups; 1-way ANOVA for the comparison of multiple groups; and 2-way ANOVA for groups with two independent variables

CRediT authorship contribution statement

Chunlu Li: Investigation, Project administration, Writing – original draft, Writing – review & editing, Data curation, Visualization, Formal analysis. Chengsi Deng: Data curation, Project administration, Software. Siwei Wang: Project administration. Xiang Dong: Data curation, Formal analysis. Bing Dai: Formal analysis, Methodology. Wendong Guo: Supervision. Qiqiang Guo: Supervision. Yanling Feng: Formal analysis. Hongde Xu: Supervision. Xiaoyu Song: Formal analysis. Liu Cao: Conceptualization, Funding acquisition, Supervision.

Declaration of competing interest

Authors declare that there are no conflicts of interest.

Data availability

Data will be made available on request.

Acknowledgments

We would like to acknowledge the extensive support from all members of Key Laboratory of Medical Cell Biology, China Medical University. This work was supported by the key project of the National Natural Science Foundation 82030091 (to LC), National Key R&D Program of China 2016YFC1302400 (to LC) and Ministry of education innovation team development plan IRT_17R107 (to LC). Schematic illustration was created with BioRender.

Appendix A. Supplementary data

Supplementary data to this article can be found online at $\frac{\text{https:}}{\text{doi.}}$ org/10.1016/j.redox.2024.103059.

References

- S.P. Nobs, M. Kopf, Tissue-resident macrophages: guardians of organ homeostasis, Trends Immunol. 42 (6) (2021) 495–507.
- [2] A. Shapouri-Moghaddam, S. Mohammadian, H. Vazini, M. Taghadosi, S. A. Esmaeili, F. Mardani, et al., Macrophage plasticity, polarization, and function in health and disease, J. Cell. Physiol. 233 (9) (2018) 6425–6440.
- [3] S. Watanabe, M. Alexander, A.V. Misharin, G.R.S. Budinger, The role of macrophages in the resolution of inflammation, J. Clin. Invest. 129 (7) (2019) 2619–2628.
- [4] X. Chen, J. Tang, W. Shuai, J. Meng, J. Feng, Z. Han, Macrophage polarization and its role in the pathogenesis of acute lung injury/acute respiratory distress syndrome, Inflamm. Res. 69 (9) (2020) 883–895.
- [5] L.A. Possamai, M.R. Thursz, J.A. Wendon, C.G. Antoniades, Modulation of monocyte/macrophage function: a therapeutic strategy in the treatment of acute liver failure, J. Hepatol. 61 (2) (2014) 439–445.
- [6] E. Kyriazopoulou, K. Leventogiannis, A. Norrby-Teglund, G. Dimopoulos, A. Pantazi, S.E. Orfanos, et al., Macrophage activation-like syndrome: an immunological entity associated with rapid progression to death in sepsis, BMC Med. 15 (1) (2017) 172.
- [7] S.K. Jo, S.A. Sung, W.Y. Cho, K.J. Go, H.K. Kim, Macrophages contribute to the initiation of ischaemic acute renal failure in rats, Nephrol. Dial. Transplant. 21 (5) (2006) 1231–1239.
- [8] A.P. West, I.E. Brodsky, C. Rahner, D.K. Woo, H. Erdjument-Bromage, P. Tempst, et al., TLR signalling augments macrophage bactericidal activity through mitochondrial ROS, Nature 472 (7344) (2011) 476–480.
- [9] K. Apel, H. Hirt, Reactive oxygen species: metabolism, oxidative stress, and signal transduction, Annu. Rev. Plant Biol. 55 (2004) 373–399.

- [11] P.D. Ray, B.W. Huang, Y. Tsuji, Reactive oxygen species (ROS) homeostasis and redox regulation in cellular signaling, Cell. Signal. 24 (5) (2012) 981–990.
- [12] M. Bauer, M. Goldstein, M. Christmann, H. Becker, D. Heylmann, B. Kaina, Human monocytes are severely impaired in base and DNA double-strand break repair that renders them vulnerable to oxidative stress, Proc. Natl. Acad. Sci. U. S. A. 108 (52) (2011) 21105–21110.
- [13] L. Zannini, D. Delia, G. Buscemi, CHK2 kinase in the DNA damage response and beyond, J. Mol. Cell Biol. 6 (6) (2014) 442–457.
- [14] L. Stolarova, P. Kleiblova, M. Janatova, J. Soukupova, P. Zemankova, L. Macurek, et al., CHEK2 germline variants in cancer predisposition: stalemate rather than checkmate, Cells 9 (12) (2020).
- [15] B. Kelly, L.A. O'Neill, Metabolic reprogramming in macrophages and dendritic cells in innate immunity, Cell Res. 25 (7) (2015) 771–784.
- [16] M. Kellner, S. Noonepalle, Q. Lu, A. Srivastava, E. Zemskov, S.M. Black, ROS signaling in the pathogenesis of acute lung injury (ALI) and acute respiratory distress syndrome (ARDS), Adv. Exp. Med. Biol. 967 (2017) 105–137.
- [17] E. Rendra, V. Riabov, D.M. Mossel, T. Sevastyanova, M.C. Harmsen, J. Kzhyshkowska, Reactive oxygen species (ROS) in macrophage activation and function in diabetes, Immunobiology 224 (2) (2019) 242–253.
- [18] J.C. Rodriguez-Prados, P.G. Traves, J. Cuenca, D. Rico, J. Aragones, P. Martin-Sanz, et al., Substrate fate in activated macrophages: a comparison between innate, classic, and alternative activation, J. Immunol. 185 (1) (2010) 605–614.
- [19] J. Van den Bossche, J. Baardman, M.P. de Winther, Metabolic characterization of polarized M1 and M2 bone marrow-derived macrophages using real-time extracellular flux analysis, J. Vis. Exp. 105 (2015).
- [20] W.J. Zhong, H.H. Yang, X.X. Guan, J.B. Xiong, C.C. Sun, C.Y. Zhang, et al., Inhibition of glycolysis alleviates lipopolysaccharide-induced acute lung injury in a mouse model, J. Cell. Physiol. 234 (4) (2019) 4641–4654.
- [21] L.A. O'Neill, R.J. Kishton, J. Rathmell, A guide to immunometabolism for immunologists, Nat. Rev. Immunol. 16 (9) (2016) 553–565.
- [22] J.W. Harper, G.R. Adami, N. Wei, K. Keyomarsi, S.J. Elledge, The p21 Cdk-interacting protein Cip1 is a potent inhibitor of G1 cyclin-dependent kinases, Cell 75 (4) (1993) 805–816.
- [23] J. Xaus, M. Cardo, A.F. Valledor, C. Soler, J. Lloberas, A. Celada, Interferon gamma induces the expression of p21waf-1 and arrests macrophage cell cycle, preventing induction of apoptosis, Immunity 11 (1) (1999) 103–113.
- [24] U.S. Srinivas, B.W.Q. Tan, B.A. Vellayappan, A.D. Jeyasekharan, ROS and the DNA damage response in cancer, Redox Biol. 25 (2019) 101084.
- [25] E.U. Kurz, P. Douglas, S.P. Lees-Miller, Doxorubicin activates ATM-dependent phosphorylation of multiple downstream targets in part through the generation of reactive oxygen species, J. Biol. Chem. 279 (51) (2004) 53272–53281.
- [26] S. Rundle, A. Bradbury, Y. Drew, N.J. Curtin, Targeting the ATR-CHK1 Axis in cancer therapy, Cancers 9 (5) (2017).
- [27] P. Mlcochova, H. Winstone, L. Zuliani-Alvarez, R.K. Gupta, TLR4-Mediated pathway triggers interferon-independent GO arrest and antiviral SAMHD1 activity in macrophages. Cell Rep. 30 (12) (2020) 3972–39780 e5.
- [28] A. Hirao, Y.Y. Kong, S. Matsuoka, A. Wakeham, J. Ruland, H. Yoshida, et al., DNA damage-induced activation of p53 by the checkpoint kinase Chk2, Science 287 (5459) (2000) 1824–1827.
- [29] L. Li, D.S. Ng, W.C. Mah, F.F. Almeida, S.A. Rahmat, V.K. Rao, et al., A unique role for p53 in the regulation of M2 macrophage polarization, Cell Death Differ. 22 (7) (2015) 1081–1093.
- [30] J.C. Chambard, R. Lefloch, J. Pouyssegur, P. Lenormand, ERK implication in cell cycle regulation, Biochim. Biophys. Acta 1773 (8) (2007) 1299–1310.
- [31] N.R. Aggarwal, L.S. King, F.R. D'Alessio, Diverse macrophage populations mediate acute lung inflammation and resolution, Am. J. Physiol. Lung Cell Mol. Physiol. 306 (8) (2014) L709–L725.
- [32] D.L. Laskin, R. Malaviya, J.D. Laskin, Role of macrophages in acute lung injury and chronic fibrosis induced by pulmonary toxicants, Toxicol. Sci. 168 (2) (2019) 287–301.
- [33] S. Herold, K. Mayer, J. Lohmeyer, Acute lung injury: how macrophages orchestrate resolution of inflammation and tissue repair, Front. Immunol. 2 (2011) 65.
- [34] M. Duan, W.C. Li, R. Vlahos, M.J. Maxwell, G.P. Anderson, M.L. Hibbs, Distinct macrophage subpopulations characterize acute infection and chronic inflammatory lung disease, J. Immunol. 189 (2) (2012) 946–955.
- [35] F.E. Nwariaku, Z. Liu, X. Zhu, D. Nahari, C. Ingle, R.F. Wu, et al., NADPH oxidase mediates vascular endothelial cadherin phosphorylation and endothelial dysfunction, Blood 104 (10) (2004) 3214–3220.

[36] Y. Zhang, S. Choksi, K. Chen, Y. Pobezinskaya, I. Linnoila, Z.G. Liu, ROS play a critical role in the differentiation of alternatively activated macrophages and the occurrence of tumor-associated macrophages, Cell Res. 23 (7) (2013) 898–914.

Redox Biology 70 (2024) 103059

- [37] M.J. Morgan, Z.G. Liu, Crosstalk of reactive oxygen species and NF-kappaB signaling, Cell Res. 21 (1) (2011) 103–115.
- [38] E. Kobayashi, T. Suzuki, M. Yamamoto, Roles nrf2 plays in myeloid cells and related disorders, Oxid. Med. Cell. Longev. 2013 (2013) 529219.
- [39] J.J. Haddad, S.C. Land, Redox/ROS regulation of lipopolysaccharide-induced mitogen-activated protein kinase (MAPK) activation and MAPK-mediated TNFalpha biosynthesis, Br. J. Pharmacol. 135 (2) (2002) 520–536.
- [40] A. Oeckinghaus, S. Ghosh, The NF-kappaB family of transcription factors and its regulation, Cold Spring Harbor Perspect. Biol. 1 (4) (2009) a000034.
- [41] J. Bartkova, Z. Horejsi, K. Koed, A. Kramer, F. Tort, K. Zieger, et al., DNA damage response as a candidate anti-cancer barrier in early human tumorigenesis, Nature 434 (7035) (2005) 864–870.
- [42] J. Oh, Y.D. Lee, A.J. Wagers, Stem cell aging: mechanisms, regulators and therapeutic opportunities, Nat. Med. 20 (8) (2014) 870–880.
- [43] T. Li, Z.W. Zhou, Z. Ju, Z.Q. Wang, DNA damage response in hematopoietic stem cell ageing, Dev. Reprod. Biol. 14 (3) (2016) 147–154.
- [44] J. Smith, L.M. Tho, N. Xu, D.A. Gillespie, The ATM-Chk2 and ATR-Chk1 pathways in DNA damage signaling and cancer, Adv. Cancer Res. 108 (2010) 73–112.
- [45] Z. Guo, S. Kozlov, M.F. Lavin, M.D. Person, T.T. Paull, ATM activation by oxidative stress, Science 330 (6003) (2010) 517–521.
- [46] S. Ditch, T.T. Paull, The ATM protein kinase and cellular redox signaling: beyond the DNA damage response, Trends Biochem. Sci. 37 (1) (2012) 15–22.
- [47] J. Bartkova, N. Rezaei, M. Liontos, P. Karakaidos, D. Kletsas, N. Issaeva, et al., Oncogene-induced senescence is part of the tumorigenesis barrier imposed by DNA damage checkpoints, Nature 444 (7119) (2006) 633–637.
- [48] G. Chatzinikolaou, I. Karakasilioti, G.A. Garinis, DNA damage and innate immunity: links and trade-offs, Trends Immunol. 35 (9) (2014) 429–435.
- [49] S. Ragu, G. Matos-Rodrigues, B.S. Lopez, Replication stress, DNA damage, inflammatory cytokines and innate immune response, Genes 11 (4) (2020).
- [50] S. Pereira-Lopes, J. Tur, J.A. Calatayud-Subias, J. Lloberas, T.H. Stracker, A. Celada, NBS1 is required for macrophage homeostasis and functional activity in mice, Blood 126 (22) (2015) 2502–2510.
- [51] P. Yu, X. Zhu, J.L. Zhu, Y.B. Han, H. Zhang, X. Zhou, et al., The Chk2-PKM2 axis promotes metabolic control of vasculogenic mimicry formation in p53-mutated triple-negative breast cancer, Oncogene 40 (34) (2021) 5262–5274.
- [52] E.M. Palsson-McDermott, A.M. Curtis, G. Goel, M.A. Lauterbach, F.J. Sheedy, L. E. Gleeson, et al., Pyruvate kinase M2 regulates Hif-Ialpha activity and IL-1beta induction and is a critical determinant of the warburg effect in LPS-activated macrophages. Cell Metabol. 21 (1) (2015) 65–80.
- [53] G.M. Tannahill, A.M. Curtis, J. Adamik, E.M. Palsson-McDermott, A.F. McGettrick, G. Goel, et al., Succinate is an inflammatory signal that induces IL-1beta through HIF-1alpha, Nature 496 (7444) (2013) 238–242.
- [54] W.K.E. Ip, N. Hoshi, D.S. Shouval, S. Snapper, R. Medzhitov, Anti-inflammatory effect of IL-10 mediated by metabolic reprogramming of macrophages, Science 356 (6337) (2017) 513–519.
- [55] M. Trakala, C.F. Arias, M.I. Garcia, M.C. Moreno-Ortiz, K. Tsilingiri, P. J. Fernandez, et al., Regulation of macrophage activation and septic shock susceptibility via p21(WAF1/CIP1), Eur. J. Immunol. 39 (3) (2009) 810–819.
- [56] M. Mavers, C.M. Cuda, A.V. Misharin, A.K. Gierut, H. Agrawal, E. Weber, et al., Cyclin-dependent kinase inhibitor p21, via its C-terminal domain, is essential for resolution of murine inflammatory arthritis, Arthritis Rheum. 64 (1) (2012) 141–152
- [57] H. Yao, S.R. Yang, I. Edirisinghe, S. Rajendrasozhan, S. Caito, D. Adenuga, et al., Disruption of p21 attenuates lung inflammation induced by cigarette smoke, LPS, and fMLP in mice, Am. J. Respir. Cell Mol. Biol. 39 (1) (2008) 7–18.
- [58] J.C. Scatizzi, J. Hutcheson, E. Bickel, J.M. Woods, K. Klosowska, T.L. Moore, et al., p21Cip1 is required for the development of monocytes and their response to serum transfer-induced arthritis, Am. J. Pathol. 168 (5) (2006) 1531–1541.
- [59] H. Takai, K. Naka, Y. Okada, M. Watanabe, N. Harada, S. Saito, et al., Chk2-deficient mice exhibit radioresistance and defective p53-mediated transcription, EMBO J. 21 (19) (2002) 5195–5205.
- [60] Q.Q. Guo, S.S. Wang, S.S. Zhang, H.D. Xu, X.M. Li, Y. Guan, et al., ATM-CHK2-Beclin 1 axis promotes autophagy to maintain ROS homeostasis under oxidative stress, EMBO J. 39 (10) (2020) e103111.